

## Multispectral satellite imagery and machine learning for the extraction of shoreline indicators

Emma McAllister<sup>a,\*</sup>, Andres Payo<sup>b</sup>, Alessandro Novellino<sup>b</sup>, Tony Dolphin<sup>c</sup>, Encarni Medina-Lopez<sup>a</sup>

<sup>a</sup> The University of Edinburgh, School of Engineering, Institute for Infrastructure and Environment, EH9 3JL, UK

<sup>b</sup> British Geological Survey, Keyworth, Nottingham, NG12 5GG, UK

<sup>c</sup> Centre for Environment, Fisheries and Aquaculture, Science, Lowestoft, NR33 0HT, UK

### ARTICLE INFO

#### Keywords:

Remote sensing  
Shoreline indicators  
Shoreline extraction  
Machine learning

### ABSTRACT

Analysis of shoreline change is fundamental to a broad range of investigations undertaken by coastal scientists, coastal engineers, and coastal managers. Multispectral Satellite Imagery (MSI) provides high resolution datasets that allow coastlines to be monitored more frequently and on a global scale. The Landsat and Sentinel-2 MSI datasets are free for public use, which has increased the frequency of studies focusing on coastal change using satellite imagery. However, despite access to global and free satellite imagery, a method has yet to be developed to monitor different shoreline types and indicators globally, as not all shorelines are sandy beaches, and the waterline cannot be representative of all shoreline changes. The review paper introduces different techniques used currently to extract shoreline features, including water indexing, Machine Learning (ML) and segmentation methods. We presented here a comprehensive review of range of the methods available for shoreline extraction from MSI and discuss why some shoreline features have been identified using multispectral satellite imagery and others not. This approach helps to signal where the gaps are on the current methods for shoreline extraction and provides a roadmap of the key challenges that prevents MSI to be used for understanding shoreline changes at a global scale.

### 1. Introduction

Around 40% of the world's population lives within 100 km of the coastline, equating to 2.4 billion people (United Nations, 2017). The coastal zone is one of the most dynamic and high energy systems on Earth, where wind, waves and tides cause geophysical processes such as erosion, deposition and flooding to occur. These ongoing processes can present a serious risk to life, home security and economy, and wellbeing to the population living there. Increasing coastal erosion rates due to Sea Level Rise (SLR) is a concern for these coastal communities. Since 1900, sea level has risen 16 cm in the UK (Environment Agency, 2020) and by 20 cm globally, with the average rate of SLR being  $3.7 \text{ mm yr}^{-1}$  between 2006 and 2018 (IPCC et al., 2021). Athanasiou et al. (2020) projected that for Europe, SLR creates a median shoreline retreat of 97 m (under RCP 8.5) by 2100, translating to  $2,500 \text{ km}^2$  of coastal land loss. The threat of increased erosion and flooding has focussed the attention of coastal practitioners and local government on shoreline change rates, the need to protect communities and the longevity and maintenance

coastal assets. It is estimated that in the European Union (EU), 1.8 to 2.9 million people could be impacted by SLR by 2050 with damage costs expected to be €135 billion to €145 billion (COACCH, 2019), including protective infrastructure and planning for mitigation.

Understanding shoreline change has traditionally utilized field studies including in situ beach profiling/surveys and aerial imagery to provide high resolution datasets for analysis (Splinter et al., 2018). Other aerial remote image-based techniques, including photogrammetry, airborne Synthetic-Aperture Radar (SAR), airborne Light Detection and Ranging Technology (LiDAR) and video imaging from drones and manned aircrafts have been used to detect shorelines, however, they are limited in terms of temporal and spatial coverage and can be costly.

The alternative is remote sensing of the earth from space, which began with the launch of Earth Observation (EO) satellites in 1972. EO satellites utilise many of the same features developed for airborne surveys, but they overcome the issues of high costs, limited spatial coverage, and low survey frequency, because EO satellite data is often free, has global coverage and regular revisit intervals. With freely

\* Corresponding author. The University of Edinburgh, School of Engineering, gb.  
E-mail address: [Emma.McAllister@ed.ac.uk](mailto:Emma.McAllister@ed.ac.uk) (E. McAllister).

available satellite imagery, the ability to monitor the coastline from space on a regular basis becomes possible. With this wealth of satellite imagery, the number of scientific publication and commercial products attempting to extract shoreline from space has radically risen (e.g., García-Rubio et al., 2015; Lira and Taborda, 2014; Hagenaaers et al., 2018; Splinter et al., 2018; Luijendijk et al., 2018; Mentaschi et al., 2018; Vos et al., 2019a; Rogers et al., 2021).

In order to monitor coastal change from satellites up to a global scale, the shoreline definition and an accurate extraction method must be determined. Various coastal features can be identified as ‘indicators’ or ‘proxies’ of the true shoreline position (the extracted waterline which has been corrected to the intersection of a tidal datum, e.g., Mean Sea Level (MSL)), whereas shoreline indicators are proxies’ representative of the entire coastline. The most identified shoreline indicator from MSI is the instantaneous waterline, as it is the most visually discernible feature (Xu, 2018; García-Rubio et al., 2015). Most extracted shorelines need to be tidally corrected if they are to be consistently used to monitor shoreline change. Tidal datum-based shoreline features are contours which have been translated horizontally based on the known elevation of the mean sea level along the shoreline (e.g., Mean High Water Line (MHWL)). They’re the most difficult features to extract from multi-spectral satellite imagery, as these indicators rely on additional data, such as time and tidal elevation (Esmail et al., 2019). Therefore, shoreline datasets are not always comparable, as they depend on how the user defines the indicator and method applied to extract it. It is essential to be able to monitor shoreline change on local to global scales, as sea level rise impacts the entire coastal system and shoreline dynamics. Satellite imagery is suitable for this type of analysis as it provides a global coverage and has a large historical database of imagery. Another major focus in shoreline studies is the methodology to extract these shoreline indicators. Many delineation and classification methods have been applied to remote sensing imagery to extract the shoreline position, including manual extraction, water indexing techniques and ML. Whilst it is easy to apply these techniques to small scale studies (<100 km) and produce highly accurate results, on a global scale the application needs to be considered and automated processing methods to be utilized (owing to the large spatial scale).

Compared to previous review papers focusing on shoreline identification and extraction using all types remote sensing methods (Boak and Turner, 2005; Toure et al., 2019; Turner et al., 2021), this paper reviews previous EO studies used for mapping shoreline indicators from MSI. As part of the review, we also analyse how recent emerging processing technologies (e.g., Machine Learning - ML or Artificial Intelligence) can be considered in new ways to extract different features from local to global scales. The benefits and drawbacks of ML technologies are discussed to identify gaps opening a new area of coastal research and techniques suitable for EO.

The paper is structured as follows: Section 2 discusses the definition of coastal indicators and how they are used to identify features along the coastline. Section 3 provides an overview of the most popular satellite data for detecting shoreline indicators, whilst Section 4 describes the main techniques used for extracting shoreline indicators from satellite data. However, as this paper is focused on reviewing the initial identification of these indicators from satellite imagery and not the shoreline derived from post processing, these secondary steps have not been included. Section 5 shoreline identification and extraction methods and presents gaps in the science of shoreline extraction from satellite imagery, whilst Section 6 concludes the findings of this paper.

## 2. Shoreline indicators

The shoreline is defined Boak and Turner (2005) as the physical interface between the land and water. This interface constantly changes over time due to water level and land fluctuations (waves, tides, weather, erosion, accretion), making it somewhat difficult to define a single, moderately static feature that represents the land and how it is

physically changing, even over very short periods. Consequently, a consistent shoreline definition is critical in order to attempt to avoid inconsistencies or capture uncertainty to minimise it, between different shoreline positions and the potential for misleading erosion/accretion results that may be methodological rather than real (Liu, 2009). Shoreline indicators are visual features used as a proxy to represent the shoreline position; these can be split into three groups:

- **Visually discernible coastal features** are features which can be physically seen and manually digitized, such as the previous high-water line (HWL) or the wet/dry boundary.
- **Tidal datum-based shorelines**, comparative to the true shoreline position are based on tidal datums (the standard elevation defined by a stage of the tide) determined by the intersection of the coastal profile with a specific vertical elevation. Proxies of tidal datum-based shorelines include the mean high waterline (MHWL) which depends on an extracted waterline contour and tidal datum-based data.
- **Indicators based on image processing techniques** define the shoreline by applying processing techniques such as spectral enhancement (e.g., spectral unmixing algorithm, focal analysis, convolutional filters), geometric enhancement (e.g., adaptive smoothing, edge detection and enhancement) or transformations (e.g. Principal Component Analysis)) to extract proxy shoreline features from digital images, which are not visible to the human eye.

The way in which these shorelines are derived can also lead to inconsistencies in the results, as every user defines them differently or has their own interpretation of the shoreline indicator for the specified method. Identifying these features can be difficult using MSI as a wide variety of shoreline indicators exist but are not always visible on a 2D multispectral image which can be based on geomorphologic aspects, such as coastal dunes, cliffs or the configuration of vegetation along the backshore. Comparisons between indicators and also with the true shoreline, is difficult as no one indicator can be used for all types of coast as all beach profiles differ (Toure et al., 2019).

Due to the large range of shoreline indicators, an assortment of image processing tools has been used to detect shorelines in multispectral images, airborne LiDAR, SAR and video. All the features presented in Fig. 1 can be extracted using a range or combination of these image processing tools. Highlighted in red in Fig. 1 are the only shoreline indicators which can be identified using multispectral satellite imagery as they are horizontal, visual, proxy-based features which are visible in imagery with ‘coarser’ resolutions (>10 m) provided by multispectral satellite imagery compared to high resolution imagery (aerial photography). These shoreline indicators can be split into features along the shoreline, such as morphological reference lines (Bluff top/cliff top, base of bluff), vegetation limits (vegetation line, seaward edge of dune vegetation line), and wetting limits (mean high water, wet/dry line, instantaneous waterline).

## 3. Remote sensing and the shoreline

Traditionally, shorelines were (and still are) mainly monitored through the use of historical maps, aerial imagery and in situ beach profiling (Gens, 2010). The shoreline indicators described in Section 2 are visually discernible features that can all be detected using conventional photography and multispectral imaging. Some of these visually discernible features can be difficult to identify in 2D images, such as the difference between the cliff top and cliff base i.e., it may not be possible to distinguish the two if the image resolution is too coarse. These features (i.e. cliff top and base features) can be distinguished by 3D data such as SAR or LiDAR if conventional or multispectral image resolution is too low.

Tidal datum-based shoreline indicators are contours commonly identified remotely with the addition of 3D photogrammetric methods, LiDAR and SAR, as these can provide information on the vertical profile

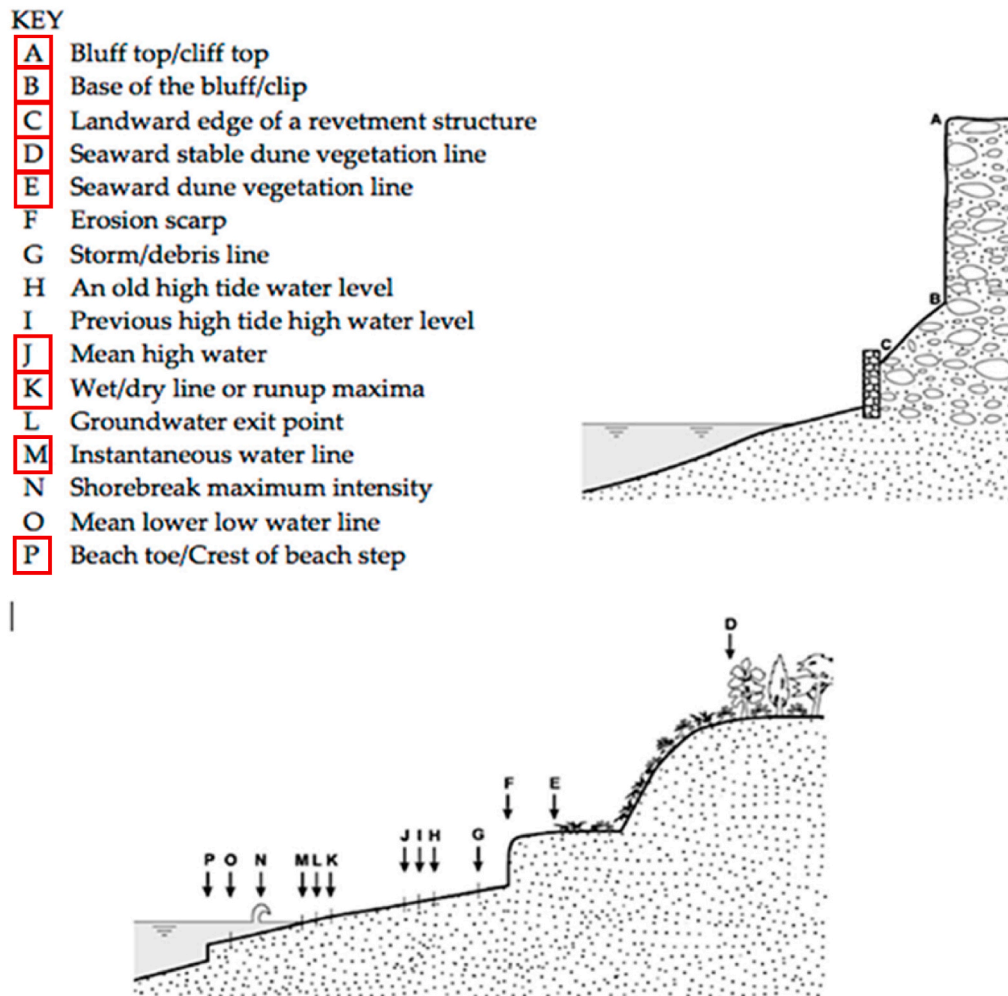


Fig. 1. Shoreline indicators (Boak and Turner, 2005). Shoreline indicators highlighted in red boxes are features which are identifiable using MSI, derived from Payo et al., (2020). (For interpretation of the references to colour in this figure legend, the reader is referred to the Web version of this article.)

of the beach. These traditional airborne techniques are effective for shoreline monitoring as they provide high resolution data used to produce accurate results on coastal change. However, 3D (topographic) data tends to be costly, labour intensive and are collected infrequently or on a relatively poor temporal resolution (compared to satellite revisits). Therefore, aerial surveys tend to be intensive for short-term studies or are regular but infrequent, missing seasonal patterns. Since the launch of Landsat-1 in 1972, the first satellite mission designed to obtain EO data (Masek et al., 2020) the potential for satellite and remote sensing techniques has increased and has been further developed alongside the intention for continuous EO with the improvement of spatial and temporal resolution. For example, spatial and temporal resolution has improved in the last two decades since the launch of Landsat-7 in 1999, Landsat-8 in 2013 and Sentinel-2, in 2015 (European Space Agency, 2017), providing more data. In 2008, the entire Landsat archive of satellite imagery (1972- present) became publicly available from USGS (Woodcock et al., 2008). The free availability of satellite data increased the number of coastal studies.

### 3.1. Multispectral satellite imagery

Multispectral satellite imagery features discrete bands across the electromagnetic spectrum, including visible light and longer wavelengths such as Near Infrared (NIR) and Shortwave Infrared (SWIR) (Ose et al., 2016). EO satellite imagery provides 50-years of historical data on a global scale and will continue to provide consistent datasets into the

future. The Landsat missions had multispectral satellite imagery from the outset and span the whole EO timeline. Fig. 2 is a timeline of the publicly and commercially available satellite imagery. The majority of the commercial satellite data comes from SPOT 1–6 (Centre National d'Etudes Spatiales) and the collection of Digital Globe satellites (WorldView, GeoEye, QuickBird, IKONOS) (Maxar, 2020). The commercial satellite missions provide 'tasked' acquisitions of imagery over specific regions of interest for the customer, typically at higher (than freely available EO satellites) resolutions of <5 m. As highlighted, with the increase of satellites being launched, there has been a corresponding increase in the temporal (revisit period) and spatial scale (pixel size). Accordingly, this review will focus on these satellites to understand their capabilities for identification and extraction of shoreline indicators over different spatial and temporal scales.

Landsat is the world's longest and continuously acquired collection of medium resolution satellite data with over four decades of data from 1972 to the present day (U.S. Geological Survey, 2016). Since the launch of Landsat-1 in 1972, six missions have been successfully launched (Landsat 2/3/4/5 MSS, Landsat-7 ETM+, Landsat-8 OLI/TIRS), (U.S. Geological Survey, 2016). Landsat-7 has been providing users with satellite data since its launch in 1999, with its higher spatial resolutions of 30 m compared to its predecessors Landsat 1–5 (resolutions of 60 m). This acquisition of higher resolution satellite imagery has been continued with the launch of Landsat 8 in 2013 which increased the number of bands available. Landsat-9 is the latest mission which was launched in September 2021 (U.S. Geological Survey, 2019). The

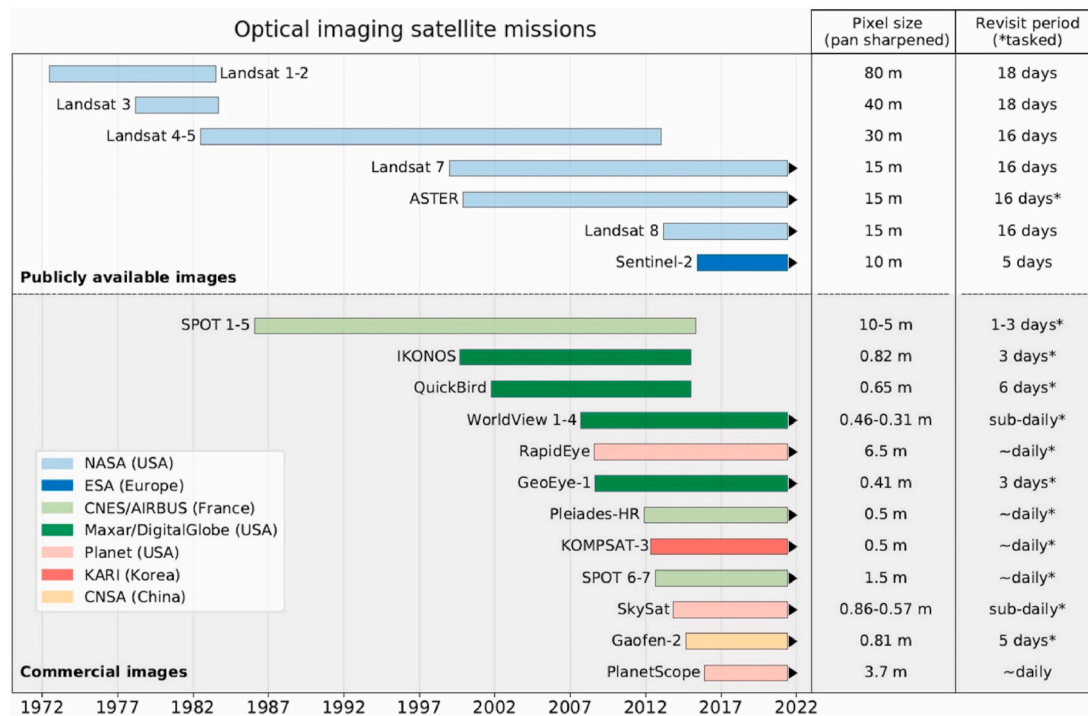


Fig. 2. Timeline of publicly available and commercial satellite imagery (Turner et al., 2021).

sensors on-board Landsat-9 are improvements on those deployed on Landsat-8, which itself provides radiometric and geometric improvements compared to the older Landsat missions. Since 2020, Landsat-9 is in the current orbit of Landsat-7, which will subsequently be decommissioned. Landsat-9 has a resolution of 30 m and is imaging the Earth every 16 days in an 8-day offset with Landsat-8 collecting up to 750 scenes per day (Masek et al., 2020). Along with Landsat-8, the two satellites will add nearly 1,500 new scenes a day to the USGS Landsat archive (U.S. Geological Survey, 2019).

Sentinel-2 is a multispectral high-resolution imaging mission managed by European Space Agency (ESA) that encompasses two twin satellites, Sentinel-2A (launched in 2015) and Sentinel-2B (launched in 2017), which are phased at 180° from each other and results in a high revisit time of five days (European Space Agency, 2017). Sentinel-2 provides a continuity of Landsat and SPOT imagery and contributes to ongoing multispectral observations that can be used for EO purposes such as landcover changes (Novellino et al., 2021).

#### 4. Shoreline extraction techniques

A wide range of techniques have been developed to extraction shorelines from georeferenced satellite imagery, this section summaries the classification techniques for the extraction of shoreline indicators from satellite imagery in Table 1 and examined/critiqued in Section 4.1, whilst Section 4.2 details how the classification/extraction techniques are used, to provide an understanding of the relationships between the shoreline indicators, the extraction methods and the satellite imagery used.

##### 4.1. Identification and extraction of coastal indicators

Numerous shoreline indicators (proxies for the 'true' shoreline) have been developed (Fig. 1), however only some of those presented in Table 1 can be extracted from satellite imagery (Payo et al., 2020). The shoreline features that can be extracted from satellite imagery are: wetting limits, vegetation limits and morphological lines, which relate to the visually discernible coastal features discussed in Section 2.

As shown in Table 1, the most common indicator is the instantaneous waterline (62%). Morphological reference lines and vegetation limits from multispectral satellite images are much less commonly used as shoreline indicators, due to the indicators requiring higher resolution imagery. After the extraction of the shoreline, indicators are usually corrected to a known tidal datum-based shoreline using auxiliary data to remove/minimise the tidal signal in the data and allow direct comparison. Many of the extracted waterlines have not been further corrected once extracted (Luijendijk et al., 2018; Bishop-Taylor et al., 2019) and are validated against other shoreline positions, which have been carried out visually (Luijendijk et al., 2018; Sunder et al., 2017; Pardo-Pascual et al., 2012; Ge et al., 2014), using in situ data, or using vertical profile data (Vos et al., 2019a; Xu, 2018; Sekovski et al., 2014; García-Rubio et al., 2015; Hagenaars et al., 2018). Other studies focus on developing and testing new extraction methods by comparison with shorelines from other studies and focusing on method validation rather than accuracy of the results (e.g., Li et al., 2018; Liu et al., 2019; Manaf et al., 2018).

The most common shoreline extraction techniques for the instantaneous waterline shoreline indicator are the indexing methods (Section 4.2.1), including the Normalized Difference Water Index (NDWI) (Gao, 1996; McFeeters, 1996) and the Modified Normalized Difference Water Index (MNDWI) (Xu, 2006). Recently ML techniques have become popular for the extraction the instantaneous waterline (see Section 4.2.3), based on pixel classification. The NDWI/MNDWI has also been used alongside ML classification techniques, to improve the extraction process (Vos et al., 2019a; Luijendijk et al., 2018) or as a comparison of the accuracy of different shoreline extraction types (Acharya et al., 2016). The land-water boundary derived from indexing methods are common and are proven to be accurate, which makes it clear why indexing methods are consistently used for the extraction of the instantaneous waterline.

The wet/dry boundary is another wetting limit which has been extracted from satellite imagery, as it is the boundary between the wet sand and the dry sand, visible after high tides. Dolan et al. (1978) highlights that the wet/dry line is a more 'stable' indicator as it isn't affected as much by the tidal stage compared to the instantaneous waterline, however as an intertidal feature the tide needs to be part way

**Table 1**

Shoreline's indicators derived from multispectral satellite images and their corresponding extraction methods modified from Payo et al. (2020) and Toure et al. (2019).

Feature e.g., tidal datums/reference lines etc	Coastal Shoreline Indicator (CSI)		Study	Shoreline extraction technique	Satellite Resolution	
Morphological limits	Coastal Dunes	Dune Crest Line	Sparavigna (2016)	Using the GIMP, Image Manipulation Program the dunes and their footprints are identified and outlined by applying the filter for the edge detection with the <b>Sobel method</b>	<10 m	
		Dune Foot	Dogru et al. (2006)	The unsupervised image classification technique <b>ISODATA (Iterative Self-Organizing Data Analysis Technique)</b> was used to identify five different land classes in satellite imagery.	>20 m	
			Merlotto et al. (2014)	Dune foot was <b>manually</b> digitized with a high-resolution scanner and georeferenced from a minimum of 15 control points.	<10 m	
	Cliffs and Backed Beach In case of Scree at the cliffs toe Protected Seafront	Base of bluff/cliff	Eguchi and Albino (2018)	The shorelines were extracted manually from the satellite imagery	<10 m	
		Landslide headwall	Scaioni et al. (2014)	<b>Visual interpretation</b> of images, including the use of stereovision.	<10 m >20 m	
		Landward edge of shore protection structure	Balaji et al. (2017)	A <b>Vectorization technique</b> is applied to obtain the shoreline in the ArcGIS 10. This is input into the <b>Digital Shoreline Analysis System (DSAS)</b> tool to estimate the rate of shoreline changes.	<10 m	
	Vegetation Limits	Vegetation line		Tarmizi et al. (2014)	<b>ISODATA</b> was used to identify 7 classes to effectively separate water from land features	<10 m
				Bengoufa et al. (2021a)	Remotely sensed images were processed using a <b>Convolutional Neural Network (CNN)</b> . The result was used as input data for the <b>Geographic Object Based Image Analysis (GEOBIA)</b> knowledge-based classification, which is used for segmenting geospatial imagery into meaningful image objects, and valuing their characteristics across spectral spatial, and temporal scales	<10 m
			Seaward edge of dune vegetation	Cenci et al. (2017)	<b>Geomatic-based Shoreline Analysis Method (GbSAM)</b> is applied in high energy coastal environments by exploiting Landsat images.	>20 m
		Ford (2013)	Vegetation lines were <b>manually digitized</b> by a single operator using ArcGIS 10.0.	<10 m		
		Lira and Taborda (2014)	Detection and extraction were carried out <b>manually</b> by digitizing the visible vegetation line in ArcGIS 10.1	>20 m		
Instant tidal levels and wetting limits	Instantaneous Waterline		Rogers et al. (2021)	A <b>CNN, VEdge_Detector</b> was used for the automated detection of coastal vegetation edges by producing a heatmap, showing the pixels predicted with the highest confidence the vegetation line.	<10 m	
			Sunder et al. (2017)	The waterline was extracted using the <b>Normalized Difference Water Index (NDWI), Modified Normalized Difference Water Index (MNDWI), Automatic Water Extraction Index (AWEI)</b> with a <b>threshold</b> used to create a binary image of land-water.	>20 m	
			Luijendijk et al. (2018)	Sandy beaches are detected by applying <b>Classification and Regression Trees (CART)</b> and the OSM Global transect system to identify the 'sandy transects'. Annual composite images are used to estimate the NDWI with the <b>Canny edge detection filter</b> and <b>thresholding</b> used to roughly estimate the position of the water-land transition.	10 m - <20 m	
			Xu (2018)	The <b>MNDWI</b> and the <b>zero threshold</b> was applied to create a binary image of the land and water.	<10 m	
			Hagenaars et al. (2017)	The waterline position is extracted using the NDWI and <b>Otsu's automatic threshold</b> . A <b>region growing algorithm</b> clusters the binary land-water image distinct water and land regions.	>20 m 10 m - <20 m	
			Hagenaars et al. (2018)	The <b>NDWI</b> was used to extract the shoreline position, with <b>Otsu thresholding</b> used to find the optimal threshold value from the NDWI histogram. The <b>region growing</b> algorithm was used to cluster pixels identified as water into a coherent water mask.	>20 m 10 m - <20 m	
			Choung and Jo. (2017)	A classification map was generated by the <b>Support Vector Machine (SVM)</b> and then the second binary image was generated from the coastal-surface classification map by grouping the land (rock, vegetation) and water features. A binary image separating the land and water features was generated using the NDWI and an <b>adaptive thresholding</b> method.	<10 m	
			Bishop-Taylor et al. (2019)	The shoreline was extracted using the NDWI, MNDWI, and AWEI. Three different thresholds were then tested: an <b>'optimal' threshold</b> , a <b>'zero' water index threshold</b> , and an <b>automatically derived threshold</b> .	>20 m	
			Yin and He (2011)	The <b>MNDWI</b> and <b>SVM</b> were combined for different shoreline types to create a whole shoreline. The MNDWI extracts the	>20 m	

(continued on next page)

Table 1 (continued)

Feature e.g., tidal datums/reference lines etc	Coastal Shoreline Indicator (CSI)	Study	Shoreline extraction technique	Satellite Resolution
		Vos et al. (2019a)	coastline of artificial and rock coast and SVM extracts the coastline of sandy and muddy coast. The CoastSat toolkit (Vos et al., 2019b) is used to extract the shoreline position. A <b>Multilayer Perceptron (MLP)</b> segments the image into 4 classes allowing only the sand/water classes to be used when applying the <b>MNDWI</b> and <b>Otsu's histogram thresholding</b> to the image.	>20 m 10 m - <20 m
		Thanh Tung et al. (2021)	The waterline is detected using, CoastSat (Vos et al. 2019b) with a <b>MLP</b> , the <b>MNDWI</b> with <b>Otsu's automatic threshold</b> .	>20 m 10 m - <20 m
		Manaf et al. (2018)	Supervised classification approaches were used to classify land and water classes including <b>MLP</b> , <b>Artificial Neural Network (ANN)</b> , <b>Decision Tree (DT)</b> , <b>Naïve Bayes (NB)</b> , <b>K-Nearest Neighbour (KNN)</b> , and <b>SVM</b> .	>20 m
		Minghelli et al. (2020)	<b>SVM</b> classification method was compared with four other methods the <b>Euclidean Distance (ED)</b> , the <b>Spectral Angle Mapper (SAM)</b> , <b>MLC</b> , <b>SVM</b> and <b>ANN</b>	<10 m
		Almonacid-Caballer et al. (2016)	The <b>optimum threshold</b> is obtained from a <b>histogram</b> of an infrared band when water and land are both present.	<10 m
		Randazzo et al. (2020)	Binary images were created from the NIR band, and the red band based on a <b>threshold</b> between the two bands.	>20 m <10 m
		Ge et al. (2014)	The waterline position is extracted using <b>object-oriented classification</b> .	>20 m
		Bamdadinejad et al. (2021)	Image classification using <b>SVM</b> , and <b>MLC</b> was applied using the ENVI software.	>20 m
		Kalkan et al. (2013)	<b>Object Based Classification (OBC)</b> was used with the <b>NDWI</b> to separate water surfaces. This was compared to <b>SVM</b> image classification to distinguish water bodies.	>20 m
		Cheng et al. (2017)	A <b>CNN</b> , SeNet (structured edge network) was developed for the segmentation of sea-land from using a fully convolutional neural network (FCNN) based model.	<10 m
		Li et al. (2018)	A <b>CNN</b> , DeepUNet was developed for pixel level sea-land segmentation from a FCNN based model.	<10 m
		Erdem et al. (2021)	A <b>CNN</b> , WaterNet was used for shoreline segmentation. This is a <b>Conditional Generative Adversarial Network (cGAN)</b> based model	>20 m
		García-Rubio et al. (2015)	<b>ISODATA</b> was used for image classification in ERDAS software.	<10 m
		Ali et al. (2015)	The shoreline was extracted using <b>ISODATA</b> and vectorized to obtain the shoreline.	<10 m
		Chen and Chang (2009)	The shoreline was extracted using the <b>Canny edge detection algorithm</b> .	<10 m
		Al-Mansoori and Al-Marzouqi (2016)	The <b>NDWI</b> and <b>local adaptive thresholding</b> converts the image into a binary image, with the <b>Sobel edge detector</b> used to create continuous edges representing the coastline.	<10 m
	Wet/Dry Line	Sekovski et al. (2014)	The shoreline position was extracted using semi-automatic shoreline delineation using both supervised ( <b>Parallelepiped</b> , <b>Gaussian Maximum Likelihood</b> , <b>Minimum-Distance-to-Means</b> , and <b>Mahalanobis distance</b> ) and unsupervised ( <b>ISODATA</b> ) image classification techniques on satellite imagery.	<10 m
	High Water Line	Bengoufa et al. (2021b)	Based on supervised image classification, <b>Random Forest (RF)</b> and <b>SVM</b> were used within the <b>pixel-based image analysis (PBIA)</b> and <b>Object-based image analysis (OBIA)</b> approaches.	<10 m

or completely out to reveal this line, meaning that it will not be detected on every satellite overpass as the tide may be in too far. Furthermore, only Sekovski et al. (2014) have successfully extracted the wet/dry boundary from (multispectral) satellite imagery, by exploiting the different characteristics of the spectral responses of the wet and dry sand.

The vegetation line is an example of a shoreline indicator representing vegetation limits. The shoreline indicator is further inland and has a distinct difference in pixel values between the vegetation and the sand, which is highlighted in Tarmizi et al.'s (2014) simple ML vegetation line extraction. Rogers et al. (2021) developed an automatic approach for vegetation line extraction on annual – decadal scales (called VEdge\_Detector).

In comparison to the visually discernible features described,

morphological reference lines such as cliff lines are more difficult to extract with MSI due to the resolution required from the satellite imagery and the shadows created by the cliffs in the image. To overcome this, these shoreline indicators are typically extracted manually with the addition of other RS techniques, such as LiDAR, as a vertical profile can help differentiate the difference between the top and bottom of the cliff lines and is not influenced by shadow in the image.

The relationships between satellite resolution, the shoreline indicator, and the extraction technique are important. As previously mentioned, many shoreline indicators have not been extracted due to the resolution of the satellite image. It is very common that medium-high resolution satellites such as Landsat and Sentinel-2 are popular, due to free accessibility to a large historical database of imagery, which means a high level of development has occurred on medium resolution

data.

There are correlations between the techniques used for shoreline extraction and the resolution of the satellite imagery. With very-high resolution satellites, such as WorldView, GeoEye and Quickbird (<3 m), the majority of studies extract the shoreline manually, or with shallow ML techniques such as Mahalanobis distance (Sekovski et al., 2014), MLC (Minghelli et al., 2020; Bhim Upadhyaya et al., 2003) or Parallelpiped (Sekovski et al., 2014). The shoreline features extracted at this higher resolution are dune lines, vegetation lines and cliff features, as they are more discernible with the higher resolution imagery. As the resolution decreases and becomes coarser, the variety of techniques increases, to include more ML based methods, as manual extraction of shorelines with a coarse resolution becomes more difficult and tends to have a higher human error and uncertainty.

In terms of temporal resolution, the majority of studies focus on shoreline change annually, over a number of years and use a single image per year to monitor change. The satellite images used are commonly from the summer months, as there is less cloud cover present and the influence of seasonal changes is at a minimum (Rogers et al., 2021; Chen and Chang, 2009; Almonacid-Caballer et al., 2016; Vos et al., 2019a; Xu, 2018; Al-Mansoori and Al-Marzouqi, 2016). Many studies maintain a consistent interval between images over several years, usually with Landsat and Sentinel-2 satellite imagery. However, some studies do not maintain a fixed interval between images (Al-Mansoori and Al-Marzouqi, 2016), which may be due to the availability of the satellite imagery during specific seasons during the year and the cost associated with commercial imagery (Al-Mansoori and Al-Marzouqi, 2016; Lira and Taborda, 2014). The studies in Table 1 don't examine inter-annual shoreline change, except for Vos et al., 2019a and Hage-naars et al. (2018), because cloud free imagery are difficult to obtain in most coastal locations year-round, especially during the winter months and the changing of seasons when the surrounding landcover can lead to misclassifications. Reduced cloud free images during winter months in the northern and southern hemisphere and along the equator during monsoon seasons hinders the study of shoreline change during cloudy seasons, which is a fundamental limitation to optical satellite data.

There are >10 images available every month from Landsat and Sentinel-2 satellites (Hagenaars et al., 2017), so only a 10% cloud-free return is required for monthly data over the cloudy seasons, which is still higher than most in situ monitoring (typically quarterly, bi-annual or annual surveys). However, despite the potential increased sampling using satellite even during cloudy seasons, most EO studies do not focus on seasonal variability.

The scale in which shoreline features are extracted should also be explored to understand the potential of satellite imagery for a further understanding of global shoreline change trends (Fig. 3). It is clear that the majority of studies focus on local (<20 km) to regional (20–100 km) stretches of coastline, with only 20% of studies based on continental scales (Cenci et al., 2017; Bishop-Taylor et al., 2019) and 5% based on global scales (Luijendijk et al., 2018; Mentaschi et al., 2018). This could be due to the type of shoreline indicator, or the method being used for the extraction process.

Fig. 4 highlights a common pattern that indexing methods and thresholding have used consistently throughout time for shoreline extraction. In comparison, ISODATA and manual extraction are declining in recent years (since 2017), whilst SVMs, ANNs and CNNs have become increasingly popular. In terms of scale, a similar pattern is present: indexing and thresholding are consistently used from local to global scales, ISODATA and manual extraction are applied to local and regional scales (<100 km) and ML techniques are being used for larger continental to global scale studies.

Luijendijk et al. (2018) and Mentaschi et al. (2018) show how global shorelines can be extracted using satellite imagery. Luijendijk et al. (2018) focuses on the extraction of all sandy beaches, whereas Mentaschi et al. (2018) extracts the shoreline position along almost all shoreline types (rocky/sandy/gravel beaches, deltas etc), excluding locations below latitudes of 63°, due to cloud cover, snow occurrence and long polar night. Both these studies produce erosion and accretion rates on a global scale. Mentaschi et al. (2018) uses a classifier to identify whether a pixel is “land”, “water” or “seasonal tide” and produces a result based on the in-between seasonal tide. Luijendijk et al. (2018) classifies sandy beaches worldwide by initially classifying them using

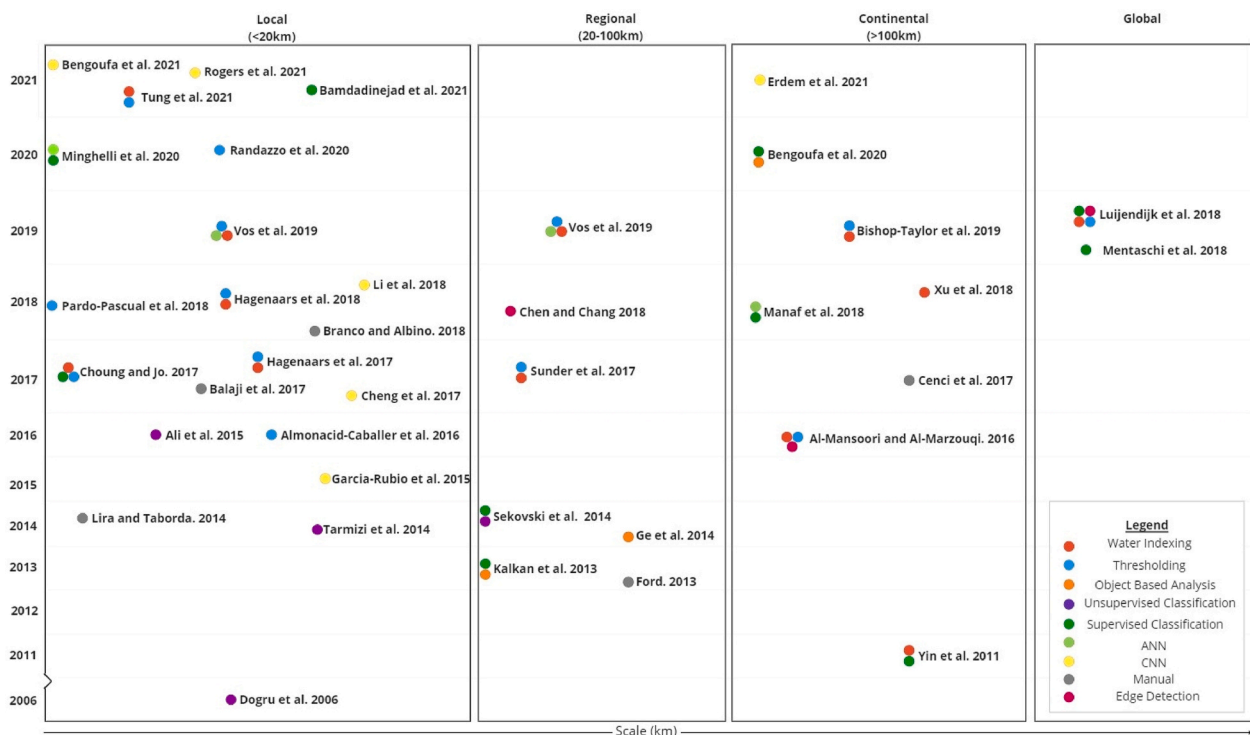


Fig. 3. Temporal scale of studies produced for shoreline extraction using MSI between 2006 and 2021.



Fig. 4. The techniques applied for shoreline extraction over scale (km) and time (years).

CART and producing a waterline using the NDWI. Although these studies were both able to create global shorelines, drawbacks are present on this scale. Mentaschi et al. (2018) had to filter out locations, with only 86% of coastlines below 63° observed. Luijendijk et al. (2018) used the NDWI on sandy beaches to extract a waterline, however the length and type of the shoreline needs to be considered as a threshold applied after the NDWI won't be representative of the area of shoreline if the surrounding coastline changes.

Shoreline type is classically dominated by sandy beaches as it is in the general scientific literature. Table 1 shows 53% of EO studies are of sandy beaches and 20% of studies are on artificial shorelines. The dominance of these two types correlates with populated study areas which are threatened by flooding and erosion or undergoing beach nourishment. There may also be a preference to sandy shorelines as their potentially higher rates of change are more easily detected in coarse satellite data over several decades, whereas rocky shores and cobble beaches are more likely to remain within a Landsat pixel over the last 50 years. By contrast, the lack of studies focusing on other shoreline features could be due to how they are commonly extracted, which may not be transferrable to satellite imagery as they are mainly extracted manually which would prove to be difficult with coarser resolutions. This leads to question whether the methodologies presented can be applied/transferred to other beach types and if the resolution of the publicly available satellites are enough for the extraction of all features, this is discussed further in Section 5.

#### 4.2. Extraction techniques

It is clear there are a variety of different techniques available for the extraction of the shoreline from MSI. These methods are mainly based on the classification of the pixel values of satellite images (PBIA) to segment the image into different features, however some studies use object-based analysis (OBIA) which integrates the spectral information of the pixels, shape, texture, and other topological features into the analysis process. From these two types of analysis, ML techniques can be applied (Kalkan et al., 2013). Alongside image classification, segmentation of the

shoreline can be carried out based on edge detection and region growing algorithms which are usually used in combination with the OBIA and PBIA. Edge detection detects and creates continuous edges in images, the most common types include the canny edge detector (Chen and Chang, 2009) and the Sobel edge detector (Carolina Sparavigna, 2013; Al-Mansoori and Al-Marzouqi, 2016). Region based segmentation divides the image into sections with similar features, where these regions contain a group of similar pixels (Hagensaars et al., 2017; Hagensaars et al., 2018).

##### 4.2.1. Water indexing

The NDWI is a band ratio technique that uses the Green and SWIR (McFeeters, 1996), or the NIR and SWIR (Gao, 1996) bands to produce greyscale images to differentiate land and water pixels, where a threshold (Section 4.2.2) between the land and water can be identified. The modified NDWI (MNDWI), replaces the NIR band with the Middle Infrared band and is used to help solve issues relating to shadows (e.g., cliffs, sea walls, buildings near the coast) in the NDWI, by increasing the contrast between water and other dark surfaces. This enhancement results in a more accurate extraction of the land-water features. The Automatic Water Extraction Index (AWEI) was introduced by Feyisa et al. (2014) to improve the accuracy of water mapping with automatic suppression of classification noise from shadows and other non-water dark surfaces. This method uses five spectral bands to enhance class separability without the need for additional data.

##### 4.2.2. Thresholding

Thresholding is widely considered to be the simplest method of image segmentation. The most common thresholding method is an automatic histogram-based technique that transforms a greyscale image, such as one created from indexing methods into a binary image (Otsu, 1979). Otsu's method can automatically derive threshold values, by iterating through all possible threshold values to calculate a measure of spread for the pixel levels on each side of the threshold value. Recently, the effectiveness of Otsu's technique has been improved by Bishop-Taylor et al. (2019), for the waterline using a subpixel approach. Other

thresholds that have been used include the ‘local adaptive’ threshold, which is obtained through trial and error. The ‘optimal’ threshold or the manually derived threshold, which represents a threshold that replicates the shoreline position, is found by iterating through a range of different thresholds for a certain beach until the derived shoreline is accurate and as close to the visible instantaneous shoreline present in the image. The ‘zero’ threshold is a constant threshold at zero that is used to extract the shoreline position, especially for large spatial extents (Bishop-Taylor et al., 2019; Sagar et al., 2017). Similar to Otsu’s automatic thresholding, Almonacid-Caballer et al. (2016) and Pardo-Pascual et al. (2012) use a thresholding technique based on the bimodal nature of a histogram of the infrared band of water and land.

4.2.3. Machine learning

Machine learning is a type of artificial intelligence that enables self-learning from data and application of its learning without the need for human intervention. ML methodologies can be applied to image classification, using algorithms that correlate pixel values within the image and input training data (made up of pixel values and corresponding class names). The more bands a satellite image has, the more data there is available for the classification with ML, which can improve the results. ML can be split into two types: supervised and unsupervised. With supervised learning, the user has full control over the training process, where the number of classes, the size of input training data, and the way the machine learns can be predefined. Whereas with unsupervised learning, the machine determines its own classes through clustering algorithms (Fig. 5), without any training data.

Fig. 5 highlights the techniques that can be used for image-based extraction. These methods can be used on their own for classification (García-Rubio et al., 2015; Hagenaars et al., 2018) or as a combination of each other (Vos et al., 2019a; Luijendijk et al., 2018). In the sections below the techniques described in Table 1 and Figs. 3 and 4 are explained as stand-alone methods, however they can be (and have been) combined to improve the overall results in identifying shoreline features. For example, Vos et al., 2019a use a combination of an MLP and

the MNDWI to allow for a more accurate analysis on sandy shorelines by reducing the chance of misclassifications (due to white-water from breaking waves and the influence of surrounding land cover).

4.2.3.1. Unsupervised machine learning. Unsupervised ML creates patterns from an image without any knowledge of labelled classes; the algorithms rely on pixels within a group to have intensities with a similar spectral pattern (García-Rubio et al., 2015). These techniques search for similarities between individual pixels and clusters of pixels and aims to find distinct features within the image (Esmail et al., 2019). The two main types of unsupervised ML methods are ISODATA and K-Means.

ISODATA (Iterative Self-Organizing Data Analysis Technique) is an algorithm that iteratively performs an entire classification and recalculates statistics. It makes use of spectrally distinctive surfaces that can identify spectral clusters effectively within satellite imagery (Ali et al., 2015). The algorithm allows the number of clusters to change from one iteration to the next, hence creating new cluster centres, which merge, or split based on a threshold determined by average intensity values between classes (Zheng and Sun, 2008). Iterations are performed with the new cluster centres which is then continued until the centre distance of the clusters fall below the defined threshold (Sekovski et al., 2014). The ISODATA algorithm is already utilized in coastal science to identify characteristics such as wet and dry sand, sand dunes and vegetation. Sekovski et al. (2014) showed that shorelines produced from ISODATA were closer to the reference shoreline positions than other methods applied for image classification.

The K- Means algorithm clusters pixel values based on their similarity. This method is very similar to ISODATA, however ISODATA statistically examines clusters after each iteration (Sekovski et al., 2014) whereas with K-Means the number of clusters are pre-defined by the user. The algorithm initially assigns each pixel to a cluster randomly and finds the centroid of each cluster. The algorithm then reiterates based on reassigning data points to the cluster whose centroid is the closest, where a new centroid for each cluster is then calculated. This iteration continues until variation between the classes cannot be reduced any

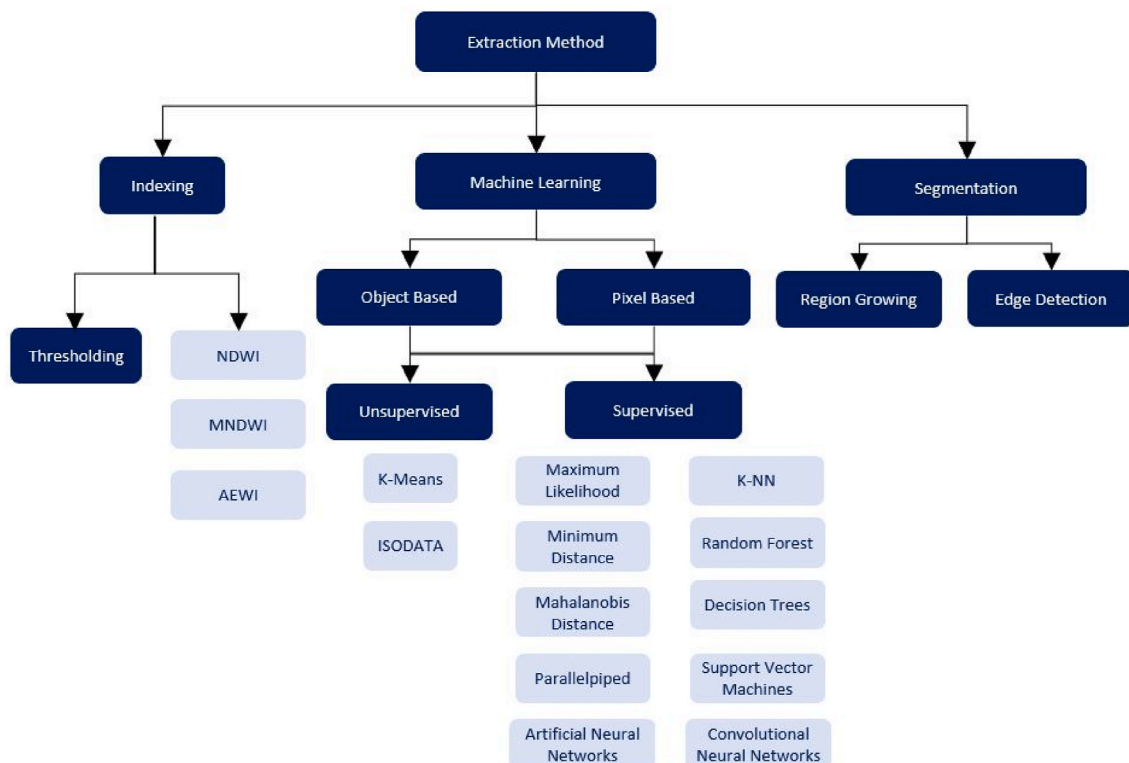


Fig. 5. Techniques that have been used in the past which have been applied for the extraction of the shoreline (Table 1).

further (Borra et al., 2005).

**4.2.3.2. Supervised machine learning.** Supervised machine learning relies on prior knowledge of a dataset and its patterns before being applied for image classification. With supervised ML the user provides the chosen algorithm with a predefined training dataset, where the algorithm learns the patterns between the spectral values of the pixels and the output classes. The way these patterns are learnt and classified depends on the algorithm it is applied to, as described below.

**Maximum likelihood classification (MLC)** is based on Bayes theorem where a discriminant function assigns the pixels to a class with the highest probability that a pixel belongs to that class based on its spectral characteristics. Sekovski et al. (2014) shows that the wet/dry boundary from the MLC tend to be further inland than the reference shoreline positions.

**Minimum distance (MD)** is based on a decision rule that calculates the spectral distance between the measurement vector for the pixel and the mean vector for each sample. Then it assigns pixels to its associated class which have a minimum spectral distance (Thirunavkkarsu and Santhosh Baboo, 2014).

**Mahalanobis distance** is a technique similar to the minimum distance. However, here a covariance matrix is used in the equation. Variance and covariance are added so highly varied clusters lead to similarly varied classes, and vice versa. The Mahalanobis distance classification algorithm assumes that histograms of band information have normal distributions (Thirunavkkarsu and Santhosh Baboo, 2014).

The **parallelepiped** algorithm defines dimensions based on the mean and standard deviation thresholds (minimum and maximum limits of class). The decision rules for assigning a class to a pixel is determined by the regions that span the range of pixel values of each class. If a pixel does not satisfy any of the classification criteria, it is left unclassified. The parallelepiped algorithm is a computationally efficient method for classifying remote sensing data as it provides simple decision boundaries. However, similarities between results for the parallelepiped algorithm and the MLC are found in Sekovski et al. (2014), as the waterline results were further from the reference waterline than other tested methods. Other errors come from gaps between parallelepipeds, where pixels within the region remain unclassified (Thakur and Maheshwari, 2017), while comparative overlap between training pixels may also exist (Perumal and Bhaskaran, 2010).

**K-Nearest Neighbour (K-NN)** is a simple concept, which assumes that similar pixels close in proximity are likely to belong to the same class. In this method, an unknown pixel is labelled by examining the training pixels and choosing the class that is most represented among a specified number of nearest neighbours (Richards and Jia, 2005). K-NN can be effective especially when the boundaries between the classes are clearly distinguished (Ose et al., 2016). This is beneficial for the extraction shoreline features such as the instantaneous waterline where the spectral values of the land and water are easily distinguishable, e.g., in clear water and white sand compared to turbid water and darker sand combinations.

**Decision tree (DT)** classification is a supervised technique where the training data is repeatedly split depending on whether a value is above or below a threshold that defines the nodes in the decision tree (Maxwell et al., 2018). **Classification and regression tree (CART)** is a common decision tree growing algorithm. The classifier is trained using a predefined dataset, which includes the number of classes and the corresponding pixel values for the different bands in the image. The classifier creates a decision tree structure based on how the training data corresponds to each class (e.g., Novellino et al., 2020). Luijendijk et al. (2018) used CART to identify sandy beaches globally, as it resulted in the lowest omission error (false negatives) and highest percentage of the positives.

**Support Vector Machines (SVM)** find the best line in two dimensions or the best hyperplane in more than two dimensions in order to separate space into classes, where the hyperplane/line is found

through the maximum distance between data points of both classes. SVM is a well-known method for identifying coastal features with different spectral-reflectance characteristics (Choung and Jo, 2017).

**Artificial neural networks (ANNs)** are statistical learning algorithms that are inspired by properties of the biological neural networks in the brain. Neural networks consist of a network of neurons which passes signals to each other. They are trained by initially assigning 'random' values for the weights of the neurons, which are then adjusted when the data is backpropagated through the network. These adjustments are based on the error associated with the output nodes. This training of the network is repeated until the error of the output is reduced to a minimum (Maxwell et al., 2018). ANNs can be simple networks made up of a single hidden layer, or contain multiple hidden layers (MLP), as the more layers are added to an ANN, the deeper the network becomes, and more complex problems can be solved.

**Multilayer Perceptron's (MLP)** are a class of feedforward ANN. CoastSat (Vos et al., 2019b) highlights the benefits of using a MLP for shoreline identification as it combines a Multi-layer Perceptron (MLP) with the MNDWI. The MLP is trained identify four landcover features (water, sand, white-water and other) from the pixel values of an input satellite image. This methodology is beneficial for shoreline extraction as it removes values from surrounding pixels relating to vegetation, buildings, roads, rocky headlands, etc, when the classification needs to only focus on the land/water classes. A similar process was carried out by Luijendijk et al. (2018), however CoastSat improved the results, with a 60% reduction in the Root Mean Square Error (RMSE). Manaf et al. (2018) highlights that in comparison to other ML methods the MLP-ANN was the most effective classifier for identifying the instantaneous waterline, achieving the highest overall accuracy compared to other ML algorithms but identifies issues relating to high training and testing times.

**Convolutional Neural Networks (CNNs)** are a ML classification technique that relies on both spatial and spectral components, providing more accuracy than ANNs. They consist of a series of layers including convolutional layers, pooling layers, and fully connected layers (Cheng et al., 2017). In recent years, they have received increased attention as they can effectively identify edges in a satellite image, as the value of the pixel of interest and neighbouring pixels are considered, which doesn't occur using traditional ML techniques (Rogers et al., 2021).

## 5. Discussion

Section 4 highlights the relationships between satellite imagery and techniques used for shoreline extraction in terms of spatial resolution, temporal resolution, and scale. From our analysis, there is a no "one size fits all" technique for the problem of extracting shoreline indicators from MSI, however ML and Neural Network analysis can be helpful reducing the number of options and help move towards a more standardized approach for all time and spatial scales. For further development of the extraction of shoreline indicators using MSI, two key factors need to be considered: the spatial and temporal scales at which the shoreline indicator is analysed, and the data source.

The extraction of the shoreline indicator is crucial as it provides a recognizable and comparable proxy for the shoreline position. There are many reasons why there is no "one size fits all" indicator for regional to global shorelines, the most important of which are different shoreline types along the coastline, which require different extraction techniques based on the morphology and composition of the shoreline (Yin and He, 2011), and where a certain shoreline indicator may not exist or be visible on certain geological/geomorphological settings (e.g cliff lines, vegetation lines, dune lines) (Ruggiero et al., 2003). Indicating that there is not one consistent shoreline indicator that can be applied universally, to represent the overall change of the shoreline, because a single shoreline indicator cannot be representative of the world's entire coastal system. An example of how this is depicted in shoreline research is through the majority of studies (53%) focusing on the extraction of the

waterline along sandy beaches (Vos et al., 2019a; Luijendijk et al., 2018; Hagenaaers et al., 2017, 2018; Sekovski et al., 2014), where there is a clear land-sea interface despite, only 31% of global coastlines being represented by sandy beaches (Luijendijk et al., 2018). The different shoreline types need to be quantified and the associated/best indicator for each shoreline type needs to be identified to represent a continuous shoreline.

A factor to consider is the visibility of the shoreline indicator in the satellite image. As previously mentioned throughout Section 4, shoreline indicators such as landslide headwalls and cliff lines may not be visible on free satellite imagery due to the lower resolution. To further this, these types of indicators may not be feasible for extraction if the scale of erosion is smaller than the resolution of a pixel within the image which is a limitation for the comprehensive freely available EO data. The visible identification of the shoreline indicator could potentially be solved by using higher resolution commercial imagery, although the records are shorter, and their availability and cost can represent a barrier. Chen et al. (2004) highlights that higher resolution satellite data may improve visibility, but this does not necessarily equate to an improvement in image classification. For example, for shoreline indicators such as the instantaneous waterline, medium to very high-resolution imagery can delineate a boundary line between pixels, as the spectral values between the two features are varied. When identifying smaller features on a very high-resolution image, such as the wet/dry boundary, the spectral values need to be taken into consideration. When the spectral values are similar, (e.g. wet/dry boundary), a speckle effect in the classification is more likely to occur as the resolution is too high and the pixel values for the different class types can have similar spectral values that are difficult to differentiate between. For shoreline features such as the vegetation line, higher resolution imagery is likely to be more successful, as the spectral values between the vegetation line and the sand are varied. From this, for shoreline extraction, the resolution of the satellite imagery should be considered for different shoreline indicators and their visibility.

Beaches may exhibit more than one shoreline indicator, and these can be utilized to give a more detailed representation of coastal change across the foreshore and the backshore. For example, a cliff backing a sandy beach can collapse due to coastal erosion. The collapse may not influence the waterline of the beach even though more sedimentary material has been added to the shoreline system. Comparatively, the collapse may extend past the current waterline. This would be considered accretion of the waterline if the shoreline is not analysed properly with an understanding of the entire system taken into consideration. This shows that the use of one indicator does not allow an understanding of the changes happening along the shoreline system. However, considering multiple shoreline indicators for shoreline change analysis allows for a more comprehensive assessment of changes to the beach system and its drivers. From this, the sediment budget and the shoreline dynamics can also be understood.

How shoreline indicators are obtained over different spatial scales is another consideration to be made when creating a methodology for shoreline extraction. It is known that pixel classification methods are successful at separating features over small study areas, including water indexing and thresholding. However, when considering using a single threshold value over a larger scale, a problem arises as there is not a "one size fits all" value to represent all shoreline types. By splitting the shoreline into smaller sections based on shoreline type or morphology, smaller clusters of specific shoreline types can be extracted to create a continuous collection of shorelines. This combination of extraction methods can potentially create continuous shoreline boundary lines based on different shoreline indicators while being extracted using a suitable and accurate method for global shorelines. Here Machine Learning and Deep Neural Networks have the greatest potential in the global shoreline mapping area because their accuracy opens the door to the creation of classification techniques for larger systems.

Another factor to be considered for the extraction of reliable

shoreline indicators is the seasonal variation. Many beaches change composition (e.g., from sand to gravel) between the seasons, which not only influences the visibility of the shoreline indicator, but it also influences the slope of the beach. Such changes may shift the shoreline proxy. While one method may be successful during one season/beach composition, it may not be for the remainder of the year. The same applies to sand dunes and cliffs that have vegetation present during some seasons of the year and none during others. If a shoreline indicator relies on vegetation for the extraction, then a way to make the proxy extractable during all seasons is essential for consistency, unless studies are only to focus on annual changes within a set season. Seasonal variability also needs to be considered for the extraction of the shoreline indicators as while one method may be successful during one season, it may not be for the remainder of the year due to changing spectral values which may influence thresholds or associated spectral values to shoreline features in classification methods. Indeed, this is why many studies only extract the shoreline position during the summer months. Here new methods can be developed for application for extraction during different periods of the year to correspond with the changing spectral values, this requires increased amounts of datasets required and more processing. This is important to consider as many studies don't consider the inter-annual changes. Within these periods mass amounts of erosion could be occurring and possibly due to the seasonal variability these changes aren't monitored.

Current studies for shoreline change using multispectral satellite imagery are focused on the physical, horizontal changes of the shoreline, but not the vertical changes. Vertical shoreline changes have been measured in the past by obtaining the bathymetry of the shoreline using multispectral satellite imagery (Randazzo et al., 2020) when combined with the extraction of the horizontal physical changes, a further understanding of the foreshore and how the coastal system is connected and changing can be obtained. This additional information can also be used alongside continuous shorelines where sediment inputs and outputs can be observed. With a way to obtain vertical data relevant to tidal datum-based shorelines from multispectral satellite imagery would allow users to extract a larger range of shoreline indicators with less need for data. So far this has been done by Vos et al. (2020). With more shoreline indicators obtainable from satellite imagery alone, a better understanding of our shorelines is possible.

From what has been discussed so far, a recurring factor is the need for large amounts of processing power and more deeper machine learning techniques to allow for a large-scale analysis of shorelines with the possibility of multiple shoreline indicators. While there is open access to free satellite imagery and geospatial tools through cloud computing platforms like Google Earth Engine these solutions are limited to non-commercial use and do not provide libraries on deep machine learning and neural networks techniques. This means that the data provided by Google Earth Engine needs to be exported to external applications to allow a more in-depth analysis of the image and shoreline, slowing down the potential of an automated process of extraction in exchange for more processing time and memory. Some of these applications have their limitations with the processing of Deep Neural Networks and large datasets, but these large techniques and datasets are essential as classification and extraction is moving towards these deeper networks. Not only are single techniques used but a combination of methods has begun to be used to increase accuracy however these will require more processing power and however an easier and automated application which is necessary can be created.

## 6. Conclusion

The purpose of this review was to understand how previous EO studies mapped shoreline indicators from MSI. Processing technologies (e.g., Machine Learning - ML or Artificial Intelligence) were also analysed to consider new ways to extract different shoreline features from local to global scales. The paper presented highlights the importance of

shoreline indicators in coastal studies and how they are important for a clear overview of the changes happening along the entire shoreline. This is significant as it allows for a deeper understanding of not only the changes happening along the land-water boundary, but from indicators which provide more understanding of the impacts of SLR on global shorelines, e.g., through cliff collapse and degradation of dunes.

Not one method can be used for the extraction of entire world's coastlines when considering the extraction of shoreline indicators and there is a need to trial more methods for the identification of different coastal indicators for different shoreline settings and on different scales, as the most common shoreline type in 53% of the papers analysed in this review at local scales.

The current research on the application of different methods for extracting shoreline indicators from MSI, has mainly been for the instantaneous waterline shoreline indicator. Which increases the need for other indicators to be extracted from MSI. In order to do this, we need to utilise techniques that are already developed for shoreline indicators with the developing ML technologies, to expand our capabilities of monitoring changes over different temporal and spatial scales.

It is important now to utilise the information acquired on available techniques and the freely available satellite imagery to monitoring shoreline change over a global scale to create a more automated and frequently updated method of monitoring our shorelines for understanding patterns and relationships of change and for the prediction of our future coastlines.

## Funding

The first author is partly funded by the British Geological Survey University Funding Initiative (BUFI) PhD studentship (S460).

## Declaration of competing interest

The authors declare that they have no known competing financial interests or personal relationships that could have appeared to influence the work reported in this paper.

## Acknowledgements

The authors would like to acknowledge British Geological Survey and Cefas (Centre for Environment, Fisheries and Aquaculture, Science) who have assisted in providing thoughts and ideas towards this research paper. AP and AN publish with the permission of the Executive Director, British Geological Survey (UKRI). TD contribution supported through Cefas Seedcorn DP1000.

## References

- Acharya, T.D., Lee, D.H., Yang, I.T., Lee, J.K., 2016. Identification of water bodies in a landsat 8 OLI image using a J48 decision tree. *Sensors* 16 (7). <https://doi.org/10.3390/s16071075>.
- Al-Mansoori, S., Al-Marzouqi, F., 2016. Coastline extraction using satellite imagery and image processing techniques international journal of current engineering and Technology coastline extraction using satellite imagery and image processing techniques. In: 1245| International Journal of Current Engineering and Technology, Vol. 6. Issue 4. <http://inpressco.com/category/ijcet>.
- Ali, T.A., Atabay, S., Mortula, M., Ma, R., 2015. Semiautomatic extraction of the shoreline from high-resolution satellite imagery and coastal terrain model. *Survey. Land Inf. Sci.* 74 (Issue 1), 15–21 (American Association for Geodetic Surveying).
- Almonacid-Caballer, J., Sánchez-García, E., Pardo-Pascual, J.E., Balaguer-Beser, A.A., Palomar-Vázquez, J., 2016. Evaluation of annual mean shoreline position deduced from Landsat imagery as a mid-term coastal evolution indicator. *Mar. Geol.* 372, 79–88. <https://doi.org/10.1016/j.margeo.2015.12.015>.
- Athanasios, P., Van Dongeren, A., Giardino, A., Voudoukas, M. I., Ranasinghe, R., & Kwadijk, J. (2020). Uncertainties in projections of sandy beach erosion due to sea level rise: an analysis at the european scale. 10, 11895. <https://doi.org/10.1038/s41598-020-68576-0>.
- Balaji, R., Sathish Kumar, S., Misra, A., 2017. Understanding the effects of seawall construction using a combination of analytical modelling and remote sensing techniques: case study of Fansa, Gujarat, India. *Int. J. Ocean Clim. Sys.* 8 (3), 153–160. <https://doi.org/10.1177/1759313117712180>.
- Bamdadinejad, M., Ketabdari, M.J., Chavooshi, S.M.H., 2021. Shoreline extraction using image processing of satellite imageries. *J. Indian Soc. Rem. Sens.* 49 (10), 2365–2375. <https://doi.org/10.1007/S12524-021-01398-3>, 2021, 49(10).
- Bengoufa, S., Niculescu, S., Mihoubi, M.K., Belkessa, R., Abbad, K., 2021a. Rocky shoreline extraction using a deep learning model and object-based image analysis. *Int. Arch. Photogram. Rem. Sens. Spatial Inf. Sci.* XLIII-B3–2, 23–29. <https://doi.org/10.5194/isprs-archives-xliii-b3-2021-23-2021>.
- Bengoufa, S., Niculescu, S., Mihoubi, M.K., Belkessa, R., Rami, A., Rabehi, W., Abbad, K., 2021b. Machine learning and shoreline monitoring using optical satellite images: case study of the Mostaganem shoreline, Algeria. *J. Appl. Remote Sens.* 15 (2), 026509 <https://doi.org/10.1117/1.jrs.15.026509>.
- Bhim Upadhya, M., Mr, N., Dorji, R., Bhutan, D., Madan, M., & Malekhu, G. (2003). Landslide Risk Assessment in the Rural Access Sector Guidelines on Best Practice Comments on a draft version of these Guidelines were received from Mr Bhim Upadhya and Mr Sushil Tiwari of DoLIDAR Nepal, Mr Rinchen Dorji and Mr Nil Kanta Giri of.
- Bishop-Taylor, R., Sagar, S., Lymburner, L., Alam, I., Sixsmith, J., 2019. Sub-pixel waterline extraction: characterising accuracy and sensitivity to indices and spectra. *Rem. Sens.* 11 (24), 1–23. <https://doi.org/10.3390/rs11242984>.
- Boak, E.H., Turner, I.L., 2005. Shoreline definition and detection: a review. *J. Coast Res.* 214, 688–703. <https://doi.org/10.2112/03-0071.1>. July 2005.
- Borra, S., Thanki, R., Dey, N., 2005. Clustering and unsupervised classification. In: *Remote Sensing Digital Image Analysis*. Springer-Verlag, pp. 249–266. [https://doi.org/10.1007/3-540-29711-1\\_9](https://doi.org/10.1007/3-540-29711-1_9).
- Carolina Sparavigna, A., 2013. A study of moving sand dunes by means of satellite images. *Int. J. Sci* 1 (8), 33–42. <https://doi.org/10.18483/ijsci.229>.
- Cenci, L., Disperati, L., Persichillo, M.G., Oliveira, E.R., Alves, F.L., Phillips, M., 2017. GIScience & Remote Sensing Integrating remote sensing and GIS techniques for monitoring and modeling shoreline evolution to support coastal risk management ARTICLE Integrating remote sensing and GIS techniques for monitoring and modeling shoreline evolution. <https://doi.org/10.1080/15481603.2017.1376370>.
- Chen, D., Stow, D.A., Gong, P., 2004. Examining the effect of spatial resolution and texture window size on classification accuracy: an urban environment case. *Int. J. Rem. Sens.* 25 (11), 2177–2192. <https://doi.org/10.1080/01431160310001618464>.
- Chen, W.W., Chang, H.K., 2009. Estimation of shoreline position and change from satellite images considering tidal variation. *Estuar. Coast Shelf Sci.* 84 (1), 54–60. <https://doi.org/10.1016/j.ecss.2009.06.002>.
- Cheng, D., Meng, G., Cheng, G., Pan, C., 2017. SeNet: structured edge network for sea-land segmentation. *Geosci. Rem. Sens. Lett. IEEE* 14 (2), 247–251. <https://doi.org/10.1109/LGRS.2016.2637439>.
- Choung, Y.J., Jo, M.H., 2017. Comparison between a machine-learning-based method and a water-index-based method for shoreline mapping using a high-resolution satellite image acquired in Hwado Island, South Korea. *J. Sens.* <https://doi.org/10.1155/2017/8245204>, 2017.
- COACCH, 2019. *The economic cost of climate change in Europe: synthesis report on interim results*. In: Paul, Watkiss, Jenny, Troeltzsch, Katriona, McGlade, Michelle, Watkiss (Eds.), Policy brief by the COACCH project. Published October 2019.
- Dogru, O.A., Balcik, F.B., Goksel, C., Ulugtekin, N., 2006. Monitoring coastal dunes by using remote sensing and GIS integration in northwest Turkey: a case study of Kilyos dunes. *Fresenius Environ. Bull.* 15 (9 B), 1216–1220. [https://www.researchgate.net/publication/290567191\\_Monitoring\\_coastal\\_dunes\\_by\\_using\\_remote\\_sensing\\_and\\_GIS\\_integration\\_in\\_northwest\\_Turkey\\_A\\_case\\_study\\_of\\_Kilyos\\_dunes](https://www.researchgate.net/publication/290567191_Monitoring_coastal_dunes_by_using_remote_sensing_and_GIS_integration_in_northwest_Turkey_A_case_study_of_Kilyos_dunes).
- Dolan, R., Hayden, B.P., Heywood, J., 1978. A new photogrammetric method for determining shoreline erosion. *Coast Eng.* 2 (1), 21–39.
- Eguchi, B.M.M., Albino, J., 2018. Bluff retreat induced by wave action on a tropical beach, in Espírito Santo, Brazil. *Revista Brasileira de Geofísica* 36 (4), 569–580. <https://doi.org/10.22564/RBGF.V36I4.959>.
- Environment Agency, 2020. National Flood and Coastal Erosion Risk Management Strategy for England. Environment Agency. <https://www.gov.uk/government/publications/national-flood-and-coastal-erosion-risk-management-strategy-for-england>.
- Erdem, F., Bayram, B., Bakirman, T., Bayrak, O.C., Akpınar, B., 2021. An ensemble deep learning based shoreline segmentation approach (WaterNet) from Landsat 8 OLI images. *Adv. Space Res.* 67 (3), 964–974. <https://doi.org/10.1016/j.asr.2020.10.043>.
- Esmail, M., Mahmood, W.E., Fath, H., 2019. Assessment and prediction of shoreline change using multi-temporal satellite images and statistics: case study of Damietta coast, Egypt. *Appl. Ocean Res.* 82, 274–282. <https://doi.org/10.1016/j.apor.2018.11.009>.
- European Space Agency, 2017. Sentinel 2A Data Access and Products. European Commission. <https://www.esa.int/ESA>. <https://sentinel.esa.int/web/sentinel/missions/sentinel-2/>.
- Feyisa, G.L., Meilby, H., Fensholt, R., Proud, S.R., 2014. Automated Water Extraction Index: a new technique for surface water mapping using Landsat imagery. *Rem. Sens. Environ.* 140, 23–35. <https://doi.org/10.1016/j.rse.2013.08.029>.
- Ford, M., 2013. Shoreline changes interpreted from multi-temporal aerial photographs and high resolution satellite images: Wotje Atoll, Marshall Islands. *Rem. Sens. Environ.* 135, 130–140. <https://doi.org/10.1016/j.rse.2013.03.027>.
- Gao, B.C., 1996. NDWI - a normalized difference water index for remote sensing of vegetation liquid water from space. *Rem. Sens. Environ.* 58 (3), 257–266. [https://doi.org/10.1016/S0034-4257\(96\)00067-3](https://doi.org/10.1016/S0034-4257(96)00067-3).
- García-Rubio, G., Huntley, D., Russell, P., 2015. Evaluating shoreline identification using optical satellite images. *Mar. Geol.* 359, 96–105. <https://doi.org/10.1016/j.margeo.2014.11.002>.

- Ge, X., Sun, X., Liu, Z., 2014. Object-oriented coastline classification and extraction from remote sensing imagery. *Rem. Sens. Environ.*: 18th Nat. Symp. Rem. Sens. Chin. 9158, 91580M. <https://doi.org/10.1117/12.2063845>.
- Gens, R., 2010. Remote sensing of coastlines: detection, extraction and monitoring. *Int. J. Rem. Sens.* 31 (7), 1819–1836. <https://doi.org/10.1080/01431160902926673>.
- Hagenaars, G., de Vries, S., Luijendijk, A.P., de Boer, W.P., Reniers, A.J.H.M., 2018. On the accuracy of automated shoreline detection derived from satellite imagery: a case study of the sand motor mega-scale nourishment. *Coast Eng.* 133, 113–125. <https://doi.org/10.1016/j.coastaleng.2017.12.011>.
- Hagenaars, G.S., Luijendijk, A.P., de Vries, S., de Boer, W.P., 2017. Long term coastline monitoring derived from satellite imagery. *Proc. Coast. Dynam.* 2017 <https://repository.tudelft.nl/islandora/object/uuid%3A34a0114b-5e39-4b52-9940-3a7e9f5a2982>.
- IPCC, 2021. Summary for policymakers. In: Zhai, P., Pirani, A., Connors, S.L., Péan, C., Berger, S., Caud, N., Chen, Y., Goldfarb, L., Gomis, M.I., Huang, M., Leitzell, K., Lonnoy, E., Matthews, J.B.R., Maycock, T.K., Waterfield, T., Yelekci, O., Yu, R., Zhou, B. (Eds.), *Climate Change 2021: The Physical Science Basis*. Contribution of Working Group I to the Sixth Assessment Report of the Intergovernmental Panel on Climate Change [Masson-Delmotte, V. In Press.
- Kalkan, K., Bayram, B., Maktav, D., Sunar, F., 2013. Comparison of support vector machine and object based classification methods for coastline detection. *Int. Arch. Photogram. Rem. Sens. Spat. Inf. Sci.* 40 (7W2), 125–127. <https://doi.org/10.5194/isprsarchives-XL-7-W2-125-2013>.
- Li, R., Liu, W., Yang, L., Sun, S., Hu, W., Zhang, F., Li, W., 2018. DeepUNet: a deep fully convolutional network for pixel-level sea-land segmentation. *IEEE J. Sel. Top. Appl. Earth Obs. Rem. Sens.* 11 (11), 3954–3962. <https://doi.org/10.1109/JSTARS.2018.2833382>.
- Lira, C., Taborda, R., 2014. Advances in applied remote sensing to coastal environments using free satellite imagery. *Coast. Res. Libr.* 9, 77–102. [https://doi.org/10.1007/978-3-319-06326-3\\_4](https://doi.org/10.1007/978-3-319-06326-3_4).
- Liu, H., 2009. Shoreline mapping and coastal change studies using remote sensing imagery and LIDAR data. *Lect. Notes Geoinf. Cartogr.* 297–322. [https://doi.org/10.1007/978-3-540-88183-4\\_13](https://doi.org/10.1007/978-3-540-88183-4_13).
- Liu, X.Y., Jia, R.S., Liu, Q.M., Zhao, C.Y., Sun, H.M., 2019. Coastline extraction method based on convolutional neural networks—A case study of jiaozhou bay in qingdao, China. *IEEE Access* 7, 180281–180291. <https://doi.org/10.1109/ACCESS.2019.2959662>.
- Luijendijk, A., Hagenaars, G., Ranasinghe, R., Baart, F., Donchyts, G., Aarninkhof, S., 2018. The state of the world's beaches. *Sci. Rep.* 8 (1), 1–11. <https://doi.org/10.1038/s41598-018-24630-6>.
- Manaf, S.A., Mustapha, N., Sulaiman, M.N., Husin, N.A., Hamid, M.R.A., 2018. Artificial neural networks for satellite image classification of shoreline extraction for land and water classes of the North west coast of peninsular Malaysia. *Adv. Sci. Lett.* 24 (2), 1382–1387. <https://doi.org/10.1166/asl.2018.10754>.
- Masek, J.G., Wulder, M.A., Markham, B., McCorkel, J., Crawford, C.J., Storey, J., Jenstrom, D.T., 2020. Landsat 9: empowering open science and applications through continuity. *Rem. Sens. Environ.* 248, 111968. <https://doi.org/10.1016/j.rse.2020.111968>.
- Maxar, 2020. Constellation | maxar. <https://www.maxar.com/constellation>.
- Maxwell, A.E., Warner, T.A., Fang, F., 2018. Implementation of machine-learning classification in remote sensing: an applied review. In: *International Journal of Remote Sensing*, vol. 39. Taylor and Francis Ltd, pp. 2784–2817. <https://doi.org/10.1080/01431161.2018.1433343>.
- McFeeters, S.K., 1996. The use of the Normalized Difference Water Index (NDWI) in the delineation of open water features. *Int. J. Rem. Sens.* 17 (7), 1425–1432. <https://doi.org/10.1080/01431169608948714>.
- Mentaschi, L., Vousdoukas, M.I., Pekel, J.F., Voukouvalas, E., Feyen, L., 2018. Global long-term observations of coastal erosion and accretion. *Sci. Rep.* 8 (1), 12876. <https://doi.org/10.1038/s41598-018-30904-w>.
- Merlotto, A., Bértola, G.R., Isla, F.I., Cortizo, L.C., Piccolo, M.C., 2014. Short and medium-term coastal evolution of Neococha municipality, Buenos Aires province, Argentina. *Environ. Earth Sci.* 71 (3), 1213–1225. <https://doi.org/10.1007/s12665-013-2525-6>.
- Minghelli, A., Spagnoli, J., Lei, M., Chami, M., Charmasson, S., 2020. Shoreline extraction from WorldView2 satellite data in the presence of foam pixels using multispectral classification method. *Rem. Sens.* 12 (16), 2664. <https://doi.org/10.3390/RS12162664>, 12, Page 2664.
- Novellino, A., Brown, T.J., Bide, T., Anh, N.T.T., Petavratzi, E., Kresse, C., 2021. Using satellite data to analyse raw material consumption in Hanoi, Vietnam. *Rem. Sens.* 13 (3), 334. <https://doi.org/10.3390/RS13030334>, 13, Page 334.
- Novellino, A., Engwell, S.L., Grebby, S., Day, S., Cassidy, M., Madden-Nadeau, A., Watt, S., Pyle, D., Abdurachman, M., Nurshal, M.E.M., Tappin, D.R., Kurniawan, I. A., Hunt, J., 2020. Mapping recent shoreline changes spanning the lateral collapse of Anak Krakatau Volcano, Indonesia. *Appl. Sci.* 10 (2), 536. <https://doi.org/10.3390/app10020536>.
- Ose, K., Corpetti, T., Demagistri, L., 2016. *Multispectral satellite image processing. In: Optical Remote Sensing of Land Surface: Techniques and Methods*. Elsevier Inc, pp. 58–124. <https://doi.org/10.1016/B978-1-78548-102-4.50002-8>.
- Otsu, N., 1979. Threshold selection method from gray-level histograms. *IEEE Trans. Syst. Man Cybern.* 9 (1), 62–66. <https://doi.org/10.1109/tsmc.1979.4310076>.
- Pardo-Pascual, J.E., Almonacid-Caballer, J., Ruiz, L.A., Palomar-Vázquez, J., 2012. Automatic extraction of shorelines from Landsat TM and ETM+ multi-temporal images with subpixel precision. *Rem. Sens. Environ.* 123, 1–11. <https://doi.org/10.1016/j.rse.2012.02.024>.
- Payo, A., Hennen, M., Martínez, J., Monteyes, X., Jaegler, T., Martin-Lauzer, F.-R., Jacobs, C., & Ellis, M. A. (2020). Monitoring Coastal Change from space; what end users need and what is feasible. 213–228. <https://doi.org/10.1680/cm.65147.213>.
- Perumal, K., Bhaskaran, R., 2010. Supervised Classification Performance of Multispectral Images. <http://arxiv.org/abs/1002.4046>.
- Randazzo, G., Barreca, G., Cascio, M., Crupi, A., Fontana, M., Gregorio, F., Lanza, S., Muzirafuti, A., 2020. Analysis of very high spatial resolution images for automatic shoreline extraction and satellite-derived bathymetry mapping. *Geosciences* 10 (5), 172. <https://doi.org/10.3390/GEOSCIENCES10050172>, 10, Page 172.
- Richards, J., Jia, X., 2005. *Supervised classification techniques. In: Remote Sensing Digital Image Analysis*. Springer-Verlag, pp. 193–247. [https://doi.org/10.1007/3-540-29711-1\\_8](https://doi.org/10.1007/3-540-29711-1_8).
- Rogers, M.S.J., Bithell, M., Brooks, S.M., Spencer, T., 2021. VEdge\_Detector: automated coastal vegetation edge detection using a convolutional neural network. *Int. J. Rem. Sens.* 42 (13), 4809–4839. <https://doi.org/10.1080/01431161.2021.1897185>.
- Ruggiero, P., Kaminsky, G.M., Gelfenbaum, G., 2003. Linking proxy-based and datum-based shorelines on a high-energy coastline: implications for shoreline change analyses. *J. Coast Res.* 38, 57–82. <https://www.jstor.org/stable/25736600>.
- Sagar, S., Roberts, D., Bala, B., Lymburner, L., 2017. Extracting the intertidal extent and topography of the Australian coastline from a 28 year time series of Landsat observations. *Rem. Sens. Environ.* 195, 153–169. <https://doi.org/10.1016/j.rse.2017.04.009>.
- Scaioni, M., Longoni, L., Melillo, V., Papini, M., 2014. Remote sensing for landslide investigations: an overview of recent achievements and perspectives. *Rem. Sens.* 6 (10), 9600–9652. <https://doi.org/10.3390/rs6109600>. MDPI AG.
- Sekovski, I., Stecchi, F., Mancini, F., Del Rio, L., 2014. Image classification methods applied to shoreline extraction on very high-resolution multispectral imagery. *Int. J. Rem. Sens.* 35 (10), 3556–3578. <https://doi.org/10.1080/01431161.2014.907939>.
- Sparavigna, A.C., 2016. Analysis of the motion of some Brazilian coastal dunes. *Int. J. Sci* 2 (1), 22–31. <https://doi.org/10.18483/ijsci.905>.
- Splinter, K., Harley, M., Turner, I., 2018. Remote sensing is changing our view of the coast: insights from 40 Years of monitoring at Narrabeen-colloroy, Australia. *Rem. Sens.* 10 (11), 1744. <https://doi.org/10.3390/rs10111744>.
- Sunder, S., Ramsankaran, R., Ramakrishnan, B., 2017. Inter-comparison of remote sensing sensing-based shoreline mapping techniques at different coastal stretches of India. *Environ. Monit. Assess.* 189 (6), 1–13. <https://doi.org/10.1007/s10661-017-5996-1>.
- Tarmizi, N.M., Samad, A.M., Yusop, M.S.M., 2014. Shoreline data extraction from QuickBird satellite image using semi-automatic technique. In: *Proceedings - 2014 IEEE 10th International Colloquium on Signal Processing and its Applications. CSPA*, pp. 157–162. <https://doi.org/10.1109/CSPA.2014.6805739>, 2014.
- Thakur, N., Maheshwari, D., 2017. A review of image classification techniques. *Int. Res. J. Eng. Technol* 4 (11), 1588–1591.
- Thanh Tung, T., Quang Chien, N., Xuan Tinh, D., 2021. Sand-spit evolution and inlet dynamics derived from satellite images: a case study for tien Chau inlet, Vietnam. *Lect. Eng. Civ. Eng.* 145 LNCE, 287–293. [https://doi.org/10.1007/978-981-16-0053-1\\_36](https://doi.org/10.1007/978-981-16-0053-1_36).
- Thirunavkkarsu, S., Santhosh Baboo, C.S., 2014. Performance of RGB and L base supervised classification technique using multispectral satellite imagery. *www.ijera.com*. In: *Journal of Engineering Research and Applications*, Vol. 4, 9. [www.ijera.com](http://www.ijera.com).
- Toure, S., Diop, O., Kpalma, K., Maiga, A.S., 2019. Shoreline detection using optical remote sensing: a review. *ISPRS Int. J. Geo-Inf.* 8 (2) <https://doi.org/10.3390/ijgi8020075>.
- Turner, I.L., Harley, M.D., Almar, R., Bergsma, E.W.J., 2021. Satellite optical imagery in coastal engineering. *Coast Eng.* 167, 103919. <https://doi.org/10.1016/j.coastaleng.2021.103919>.
- U.S. Geological Survey, 2019. Landsat 9. In: *Fact Sheet*. <https://doi.org/10.3133/fs20193008>.
- U.S. Geological Survey, 2016. Landsat—earth observation satellites. In: *Fact Sheet*. <https://doi.org/10.3133/fs20153081>.
- United Nations, 2017. *June. Factsheet: people and oceans. In: Proceedings of the Ocean Conference*, pp. 1–7.
- Vos, K., Harley, M.D., Splinter, K.D., Simmons, J.A., Turner, I.L., 2019a. Sub-annual to multi-decadal shoreline variability from publicly available satellite imagery. *Coast Eng.* 150 (April), 160–174. <https://doi.org/10.1016/j.coastaleng.2019.04.004>.
- Vos, K., Harley, M.D., Splinter, K.D., Walker, A., Turner, I.L., 2020. Beach slopes from satellite-derived shorelines. *Geophys. Res. Lett.* 47 (14) <https://doi.org/10.1029/2020GL088365>.
- Vos, K., Splinter, K.D., Harley, M.D., Simmons, J.A., Turner, I.L., 2019b. CoastSat: a Google Earth Engine-enabled Python toolkit to extract shorelines from publicly available satellite imagery. *Environ. Model. Software* 122, 104528. <https://doi.org/10.1016/j.envsoft.2019.104528>.
- Woodcock, C.E., Allen, R., Anderson, M., Belward, A., Bindschadler, R., Cohen, W., Gao, F., Goward, S.N., Helder, D., Helmer, E., Nemani, R., Oreopoulos, L., Schott, J., Thenkabail, P.S., Vermote, E.F., Vogelmann, J., Wulder, M.A., Wynne, R., 2008. Free access to landsat imagery. *Science* 320 (5879), 1011. <https://doi.org/10.1126/science.320.5879.1011a>. American Association for the Advancement of Science.
- Xu, H., 2006. Modification of normalised difference water index (NDWI) to enhance open water features in remotely sensed imagery. *Int. J. Rem. Sens.* 27 (14), 3025–3033. <https://doi.org/10.1080/01431160600589179>.

- Xu, N., 2018. Detecting coastline change with all available landsat data over 1986–2015: a case study for the state of Texas, USA. *Atmosphere* 9 (3), 107. <https://doi.org/10.3390/atmos9030107>.
- Yin, J., He, F., 2011. Researching the method of coastline extracted by remote sensing image. In: 2011 International Conference on Remote Sensing, Environment and Transportation Engineering. RSETE 2011 - Proceedings, pp. 3441–3444. <https://doi.org/10.1109/RSETE.2011.5965052>.
- Zheng, C., Sun, D.W., 2008. Image segmentation techniques. In: *Computer Vision Technology for Food Quality Evaluation*. Academic Press, pp. 37–56. <https://doi.org/10.1016/B978-012373642-0.50005>.

## List of Acronyms

*MSI*: Multispectral Satellite Imagery 1.0  
*ML*: Machine Learning 1.0  
*SLR*: Sea Level Rise 1.0  
*EU*: European Union 1.0  
*SAR*: Synthetic-Aperture Radar 1.0  
*LIDAR*: Light Detection and Ranging Technology 1.0  
*EO*: Earth Observation 1.0  
*MSL*: Mean Sea Level 1.0  
*MHWL*: Mean High Water Line 1.0  
*HWL*: High Water Line 2.0

*NIR*: Near Infrared 3.1  
*SWIR*: Shortwave Infrared 3.1  
*DSAS*: Digital Shoreline Analysis System 4.1  
*GEOBIA*: Geographic Object Based Image Analysis 4.1  
*GbSAM*: Geomatic-based Shoreline Analysis Method 4.1  
*NB*: Naïve Bayes 4.1  
*ED*: Euclidean Distance 4.1  
*SAM*: Spectral Angle Mapper 4.1  
*RF*: Random Forest 4.1  
*OBC*: Object Based Classification 4.2  
*PBIA*: Pixel-Based Image Analysis 4.2  
*OBA*: Object-Based Image Analysis 4.2  
*NDWI*: Normalized Difference Water Index 4.2.1  
*MNDWI*: Modified Normalized Difference Water Index 4.2.1  
*AWEI*: Automatic Water Extraction Index 4.2.1  
*ISODATA*: Iterative Self-Organizing Data Analysis Technique 4.2.3.1  
*CART*: Classification and Regression Trees 4.2.3.2  
*SVM*: Support Vector Machine 4.2.3.2  
*MLP*: Multilayer Perceptron 4.2.3.2  
*ANN*: Artificial Neural Network 4.2.3.2  
*DT*: Decision Tree 4.2.3.2  
*CNN*: Convolutional Neural Network 4.2.3.2  
*KNN*: K- Nearest Neighbour 4.2.3.2